Electronic properties of a grain boundary in Sb-doped ZnO

2001 J. Phys.: Condens. Matter 13 9937

(http://iopscience.iop.org/0953-8984/13/44/309)

INSTITUTE OF PHYSICS PUBLISHING JOURNAL OF PHYSICS: CONDENSED MATTER

J. Phys.: Condens. Matter **13** (2001) 9937–9943 PII: S0953-8984(01)27411-6

Electronic properties of a grain boundary in Sb-doped ZnO

J M Carlsson[1], B Hellsing[1], H S Domingos[2] and P D Bristowe[2]

[1] Experimental Physics, Chalmers and Göteborg University, SE-412 96 Gothenburg, Sweden
[2] Department of Materials Science and Metallurgy, University of Cambridge, Pembroke Street, Cambridge CB2 3QZ, UK

E-mail: pdb1000@cus.cam.ac.uk

Received 30 July 2001
Published 19 October 2001
Online at stacks.iop.org/JPhysCM/13/9937

Abstract

The electronic properties of a $\Sigma = 13$ 32.2° [0001] tilt grain boundary in ZnO have been investigated using first-principles calculations. Two atomic models for the boundary have been considered, one of which contains structural units that are consistent with those observed for this orientation using electron microscopy. Doping both the grain boundary models with antimony reveals a strong driving force for segregation. Analysis of the electronic densities of states, bond populations and Mulliken charges shows that antimony creates a localized impurity state in the grain boundary and acts as a donor dopant. The resulting charge accumulation at the grain boundary together with the presence of local bonds that are metallic in character, will influence the mechanism for charge transport across the interface and this is discussed in relation to varistor applications.

1. Introduction

Zinc oxide has attracted renewed interest in recent years due to the development of thin-film fabrication techniques which have extended the range of possible device applications for this wide band gap semiconductor [1]. The possibility of growing large-scale single crystals [2] has enabled the construction of blue laser diodes [3] and also electrodes for solar cells and flat panel displays [4]. Varistors are the traditional use of ZnO when the material is prepared in polycrystalline form [5]. In all applications, defects and impurities are the key factors in determining functionality. In particular, grain boundaries in polycrystalline ZnO have received much attention [6–12] because in the double Schottky barrier (DSB) model [13–16] they are considered to be the origin of the material's non-linear *I–V* characteristic, a property which is essential in varistor applications. The DSB model assumes that the grain boundary contains interface states which trap conduction electrons. This creates a depletion region close to the boundary that acts as a barrier for electron transport between adjacent grains. The breakdown

of the barrier is connected to the release of the trapped charge carriers. This breakdown may be enhanced by an avalanche mechanism [15] where holes from field-induced electron–hole pairs travel back to the grain boundary and recombine with trapped electrons.

There have been few theoretical investigations at the microscopic level to test the DSB model mainly because individual grain boundaries must be studied. Oba *et al* [17, 18] have recently used a computational approach to calculate the atomic and electronic structure of an undoped $\Sigma = 7$ [0001] tilt grain boundary in ZnO. However, no interface states were found and vacancy-induced states seem to be insufficient to explain the extreme electrical non-linearity found in commercial varistor material [19]. The structural or electrical properties of this boundary have not been determined experimentally but the atomic structure of another [0001] tilt boundary near $\Sigma = 13$ has been observed and characterized using high-resolution electron microscopy (HREM) [8, 9]. In the present paper, therefore, we have focused on the $\Sigma = 13$ tilt grain boundary as our model system and analysed its properties with and without impurities using first-principles electronic structure calculations. Antimony was chosen as the impurity since antimony oxide is a common additive in ZnO varistor ceramics [20]. The oxide additive is often observed to react with the host material to form a spinel [21] which then inhibits grain growth by residing on the grain boundaries and at triple junctions [22]. However, the effect of Sb *per se* on the atomic or electronic structure of grain boundaries and the degree to which it contributes to varistor activity are not understood. Energy-dispersive x-ray analysis has shown that Sb can be distributed in the grain boundaries, the grains and the secondary spinel phase depending on the concentration of antimony oxide in the system [23]. Our aim, therefore, is to get a clearer understanding of the effects of Sb segregation on the atomic and electronic structure of a model tilt boundary system in ZnO.

2. Computational method

The calculations are based on density functional theory (DFT) and use a supercell approach to model the grain boundary. The supercell for the $\Sigma = 13$ $32.2^\circ(13\bar{4}0)$[0001] tilt boundary system contained two symmetry equivalent boundaries and used 104 atoms. To begin with, however, the lowest energy translation states of the boundary were determined using a classical shell model and lattice relaxation techniques [24]. These calculations predicted two stable translation states for the $\Sigma = 13$ tilt boundary which were chosen for final optimization using the DFT methodology [25–27]. The two low-energy states of the boundary are labelled $\Sigma = 13_1$ and $\Sigma = 13_2$ and are shown after full relaxation in figure 1. The DFT calculations used a plane wave basis set with a kinetic energy cut-off of 300 eV, ultrasoft pseudopotentials [28], a GGA [29] exchange-correlation functional and four *k*-points selected by the Monkhorst–Pack scheme [30]. This scheme was used to calculate the total energy, the density of states (DOS), the partial DOS projected onto atomic orbitals (PDOS) and the Mulliken charges and bond populations. Figure 1 also shows the three Zn sites chosen for Sb substitution, one in the core of the $\Sigma = 13_1$ boundary and the other two in the core of the $\Sigma = 13_2$ boundary. The grain boundary E_{GB} and segregation energies E_{seg} are shown in table 1 and were determined by performing separate DFT calculations on undoped and doped bulk cells under the same computational conditions as the grain boundary calculations.

3. Results and discussion

The HREM observations [8, 9] indicate that periodic segments of a near-$\Sigma = 13$ [0001] tilt boundary are constructed from 5- and 7-atom arrangements of atomic columns (rings). Six-atom rings have also been observed in a lower angle boundary and 4- and 8-atom rings

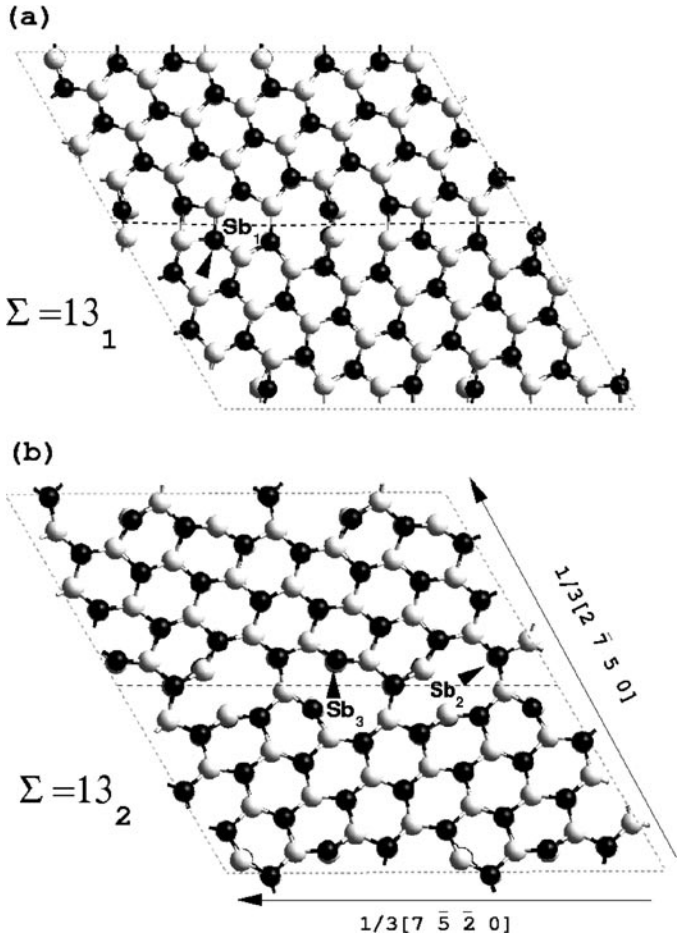

Figure 1. The two stable translation states found for the $\Sigma = 13$ grain boundary in ZnO. (a) $\Sigma = 13_1$ and (b) $\Sigma = 13_2$, both viewed down the [0001] tilt axis. Zinc atoms are shown black and oxygen atoms are shown white. The Sb substitution sites are indicated by Sb_1, Sb_2 and Sb_3. The horizontal dashed line indicates the position of the boundary plane.

have been seen in tilt boundaries of GaN [31] which has the same crystal structure as ZnO. Thus, a number of characteristic structural units are observed and their precise arrangement depends on the boundary geometry and its deviation from the ideal low-Σ configuration. Our two low-energy configurations for the $\Sigma = 13$ boundary contain all these ring structures. The lower energy boundary, $\Sigma = 13_1$, consists of a periodic array of 4-, 6-, 8- and 10-atom rings while the higher energy boundary, $\Sigma = 13_2$, comprises a zig-zag chain of 10-atom rings as seen in figure 1. The 10-atom ring is equivalent to a 5- and 7-atom ring since the bond dividing the 5- and 7-atom rings is absent due to lattice mismatch. Thus the configuration which most closely matches the HREM observations is the $\Sigma = 13_2$ structure, although we compute it to have a slightly (5%) higher energy than $\Sigma = 13_1$. The similarity in computed grain boundary energies would indicate that both geometries could coexist and this is known as structural multiplicity [32]. The preference for a particular geometry may depend on various experimental factors such as deviations from the precise coincidence site lattice misorientation, crystal stoichiometry and impurity concentration.

Table 1. The grain boundary energy E_{GB} for the two translation states of the $\Sigma = 13$ boundary and the segregation energy E_{seg} for the three substitution sites shown in figure 1.

Grain boundary	E_{GB} (J m^{-2})
$\Sigma = 13_1$	1.35
$\Sigma = 13_2$	1.42
Substitution site	E_{seg} (eV)
$\Sigma = 13_1$:Sb$_1$	−1.44
$\Sigma = 13_2$:Sb$_3$	−1.35
$\Sigma = 13_2$:Sb$_2$	0.09

The formation of structural units in the $\Sigma = 13$ grain boundary inevitably breaks the Zn–O bonds. However, the atoms in the bridge between the 8- and 10-atom rings in $\Sigma = 13_1$ are re-coordinated into a planar structure which does not have a dangling bond. Consequently, the DOS for this structure only shows a small shift and no interface states are formed. In the $\Sigma = 13_2$ boundary the broken tetrahedral bonds across the neck of the 10-atom ring (i.e. between the equivalent 5- and 7-atom rings) lead to under-coordination of the atoms in the neck positions. In particular, for the O-atoms the under-coordination produces a dangling bond directed into the interior of the 10-atom ring that can be seen as a peak in the DOS indicated by O_{GB} in figure 2(b). The PDOS for those O-atoms in figure 2(b) shows an interface state of p-character above the top of the valence band. The corresponding wave-function has a pronounced p-character localized on the O-atoms. The atoms across the neck of the 10-atom ring are found to relax inwards towards the bulk in a manner which is similar to that observed on the ZnO non-polar $(10\bar{1}0)$ surface [33]. Both the Zn and O neck atoms move into the adjacent hexagonal ring away from the more open 10-atom ring. However, the Zn-atom moves 0.01 nm further than the O-atom causing the surface of the ring to be slightly uneven. This rumpling is similar to that observed on the $(10\bar{1}0)$ surface using LEED [33]. The character of the interface state is also similar to that of a $(10\bar{1}0)$ surface state found using first-principles calculations [34]. This indicates that the under-coordinated atoms in the 10-atom ring experience the structural unit as an internal surface.

In order to understand the effects of Sb segregation on the $\Sigma = 13$ tilt boundary we have first studied Sb incorporation in the bulk crystal assuming a cation substitution mechanism. Antimony is a slightly larger atom than Zn and the substitution causes a small local outward relaxation of the nearest and next nearest neighbour atoms of about 0.01 nm due to the equilibrium length of the Sb–O bonds. The chemical effect of this substitution is the formation of a predominantly covalent bond between the Sb-atom and the four nearest neighbouring O-atoms which is in contrast to the more ionic Zn–O bond. Both the bonding and anti-bonding states of the covalent Sb–O bonds are occupied in bulk ZnO. The bonding state, indicated by the Sb-arrow in figure 2(a), has an energy of 11 eV below the Fermi level, which is lower than the energy of the d-bands from the Zn-atoms in pure ZnO. The energy of the anti-bonding Sb–O bond, indicated by Sb* in figure 2(b) is located in the band gap of ZnO with an energy of 0.24 eV above the valence band edge at the Γ-point. The location of the anti-bonding state in the band gap is unfavourable and Sb-atoms prefer to increase their distance to the nearest neighbours which explains the outward relaxation of these atoms. The PDOS shows that the covalent bond has an s–p character and we conclude that the covalent bond between the Sb-atom and the neighbouring O-atoms is formed by the 5s electrons from the Sb-atom and the 2p electrons from the O-atoms. The 5p electrons from the Sb-atom are partly donated to the conduction band as can be seen from the shift of the Fermi level in the DOS plot in

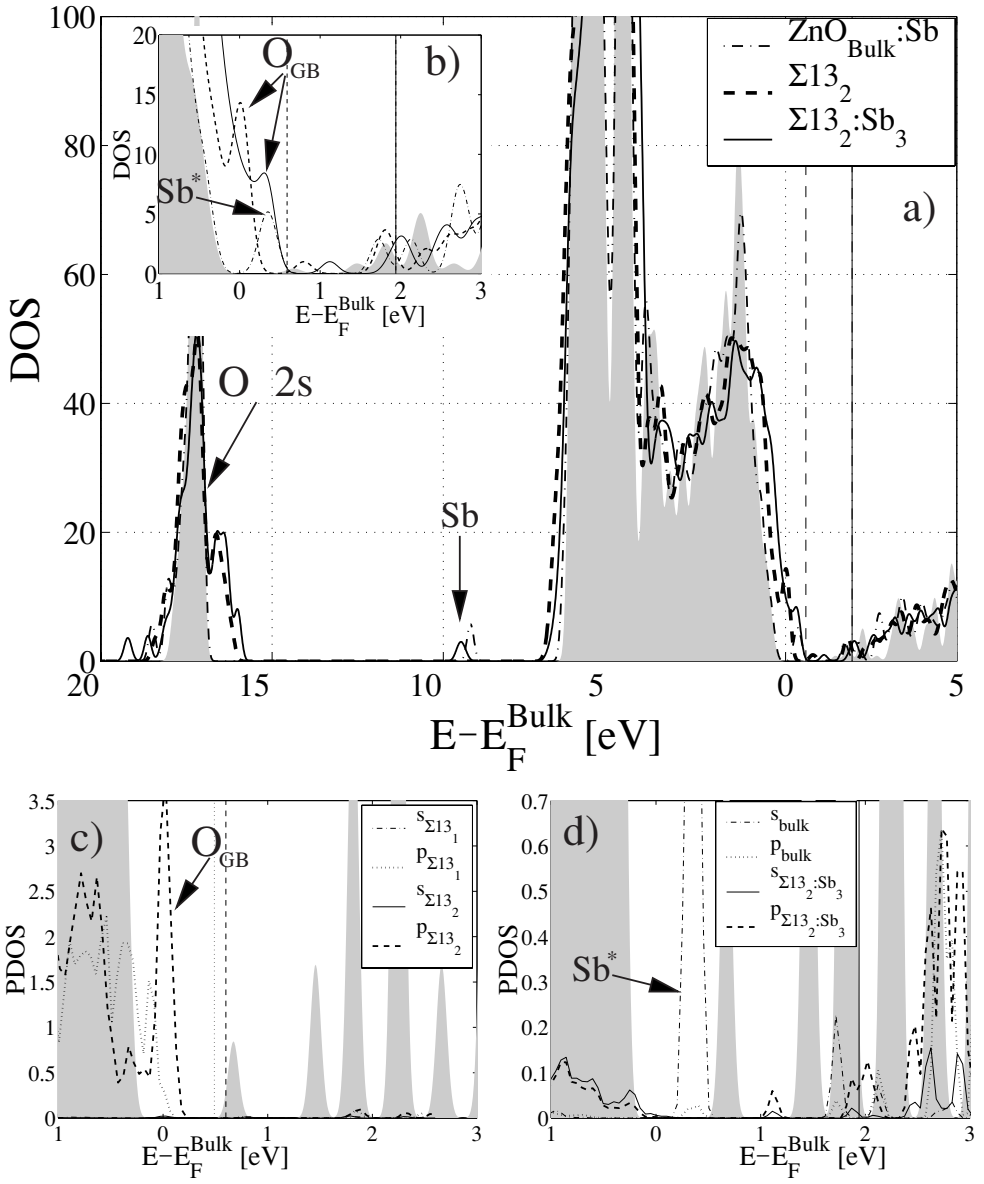

Figure 2. A comparison of the DOS for the undoped and Sb-doped bulk ZnO and $\Sigma = 13$ grain boundaries. The shaded area is the bulk DOS and the vertical dotted, dashed and solid curves indicate the position of the Fermi level in the $\Sigma = 13_1$, $\Sigma = 13_2$ and $\Sigma = 13_2$:Sb systems, respectively. (a) Sb indicates the Sb–O bonding orbital while (b) the anti-bonding orbital is labelled Sb*. The peak for the under-coordinated O-atoms in the $\Sigma = 13_2$ boundary is highlighted by O_{GB} in (b) and (c) compares the s- and p-resolved PDOS for these atoms in the $\Sigma = 13_1$ and $\Sigma = 13_2$ boundaries. (d) The relaxation of the anti-bonding Sb–O orbital in terms of the change in PDOS for the Sb-atom in moving from the bulk to the $\Sigma = 13_2$:Sb_3 site.

figure 2(a). This creates a local accumulation of charge carriers around each Sb-atom. A simple estimate of the radius of the orbital for these electrons gives a value of approximately

1.5 nm. To get a more detailed description of the effects of the Sb-induced charge accumulation we performed the Sb-substitution in an extended bulk cell. In this case a clear band bending centred at the Sb-atom is observed and the decay can be estimated. The extrapolation gives an extension of the band bending of 3 nm.

The grain boundary segregation calculations indicate that for two of the chosen substitution sites there is a strong driving force for Sb segregation. These sites are labelled Sb_1 in the $\Sigma = 13_1$ boundary and Sb_3 in the $\Sigma = 13_2$ boundary and have large negative segregation energies as shown in table 1. It is concluded that these particular sites offer more freedom for relaxation compared to the bulk crystal. In both cases the Sb-atom relaxes inwards by about 0.03–0.05 nm towards the centre of the adjacent ring structure. This is the case even though the site Sb_1 is 4-coordinated and the site Sb_3 is 3-coordinated. On the other hand, the impurity labelled Sb_2 in the $\Sigma = 13_2$ boundary has a positive segregation energy and is an unfavourable site for segregation. In this case the site that directly connects adjacent 10-atom rings, is 4-coordinated and offers little freedom for relaxation even though it is in the core of the grain boundary. It is thus a bulk-like site as far as impurity segregation is concerned. We conclude that both the models for the $\Sigma = 13$ tilt boundary can attract Sb impurities although some sites are more strongly preferred energetically than others.

We have analysed the nature of the Sb–O orbitals in the grain boundary and compared them to the corresponding orbital in the bulk. The Sb–O bonding orbitals in the bulk and the boundary have the same character while the anti-bonding orbital changes character depending on the boundary substitution site. In the 4-coordinated sites, $\Sigma = 13_1$:Sb_1 and $\Sigma = 13_2$:Sb_2, the anti-bonding state shows a distinct peak in the atom-resolved DOS, but the energy of that state is relaxed below the valence band edge. In the 3-coordinated site, $\Sigma = 13_2$:Sb_3, the anti-bonding state broadens into a less-pronounced state of a more delocalized character as can be seen in figure 2(d). The valence bond orbital around the Sb-atoms is more extended which increases the charge density inside the empty regions of the structural unit for the $\Sigma = 13_1$:Sb_1 and $\Sigma = 13_2$:Sb_3 sites. The charge density overlaps with the next nearest neighbouring Zn-atom across the structural unit but the Sb–Zn overlap does not form a bond. A Mulliken population analysis on the atoms and bonds around the $\Sigma = 13_1$:Sb_1 and $\Sigma = 13_2$:Sb_3 sites shows clear evidence of anti-bonding between Sb–Zn atoms. For example, near the $\Sigma = 13_1$:Sb_1 site the Sb–Zn bond population is -0.35 electrons whereas the Sb–O bond population is +0.65 electrons. As with the doped bulk, 5p electrons are partly donated to the conduction band when the Sb-atom occupies a boundary site. This results in an upshift of the Fermi level in the $\Sigma = 13_2$:Sb_3 system (indicted by the vertical solid line in figure 2(a)) of about 1.3 eV from the position in the undoped $\Sigma = 13_2$ grain boundary (marked by the vertical dashed line in figure 2(a)). The segregation of Sb-atoms then suggests that there is a higher concentration of charge carriers in the grain boundary region compared to the bulk. Our results indicate a 2D grain boundary interface that is more metallic in character than the interior of the grains for the doping levels that can occur in varistor materials. On the other hand, for conduction perpendicular to the grain boundary the charge accumulation may act as a repulsive barrier.

4. Conclusions

To conclude, we have analysed the electronic structure of two atomic models for the $\Sigma = 13$ [0001] tilt grain in ZnO and found that under-coordinated oxygen atoms in one of the structures creates occupied interface states just above the valence band edge. Doping this structure with Sb reveals a strong driving force for segregation which can be explained in terms of the relaxation of the Sb–O anti-bonding orbital. Antimony donates 5p electrons to the conduction

band causing charge accumulation in the grain boundary. Our results therefore indicate a varistor mechanism in which charge carriers are frozen into the grain boundary region and only released upon application of a critical external field. Further investigations concerning the transport properties of such a boundary have to be performed in order to determine whether this mechanism is quantitatively compatible with the non-linear *I–V* characteristics found for commercial varistors.

Acknowledgments

JC has been supported by the Swedish Natural Science Research Council and HSD acknowledges grant PRAXIS XXI/BD/13944/97. The calculations were performed using the CSAR and UNICC resources. The authors would also like to acknowledge useful discussions with Professor M C Payne.

References

[1] Look D C 2001 *Mater. Sci. Eng.* B **80** 383
[2] Look D C, Reynolds D C, Sizelove J, Jones R, Witton C, Cantwell G and Harsch W 1998 *Solid State Commun.* **105** 399
[3] Reynolds D C, Look D C and Jogai B 1996 *Solid State Commun.* **99** 873
[4] Ginley D S and Bright C 2000 *MRS Bull.* **25** 15
[5] Greuter F and Blatter G 1990 *Semicond. Sci. Technol.* **5** 111
[6] Olsson E and Dunlop G 1989 *J. Appl. Phys.* **66** 3666
[7] Olsson E and Dunlop G 1989 *J. Appl. Phys.* **66** 4317
[8] Kiselev A, Sarrazit F, Stepantsov E, Olsson E, Claeson T, Bondarenko V, Pond R and Kiselev N 1997 *Phil. Mag.* A **76** 633
[9] Sarrazit F, Pond R and Kiselev N 1998 *Phil. Mag. Lett.* **77** 191
[10] Mukae K and Tanaka A 2000 *Ceram. Int.* **26** 645
[11] Tanimura J, Wada O, Kurokawa H, Furuse N and Kobayashi M 2000 *Japan. J. Appl. Phys.* Part 1 **39** 4493
[12] Ohbuchi Y, Kawahara T, Okamoto Y and Morimoto J 2001 *Japan. J. Appl. Phys.* Part 1 **40** 213
[13] Mahan G D, Levinson L and Philipp H 1979 *J. Appl. Phys.* **50** 2799
[14] Blatter G and Greuter F 1986 *Phys. Rev.* B **33** 3952
[15] Blatter G and Greuter F 1986 *Phys. Rev.* B **34** 8555
[16] Mukae K 1997 *Key Eng. Mater.* **125–126** 317
[17] Oba F, Tanaka I, Nishitani S, Adachi H, Slater B and Gay D 2000 *Phil. Mag.* A **80** 1567
[18] Oba F, Nishitani S, Adachi H, Tanaka I, Kohyama M and Tanaka S 2001 *Phys. Rev.* B **63** 045410
[19] Oba F, Adachi H and Tanaka I 2000 *J. Mater. Res.* **15** 2167
[20] Matsuoka M 1971 *Japan. J. Appl. Phys.* **10** 736
[21] Agarwal G and Speyer R F 1997 *J. Mater. Res.* **12** 2447
[22] Senda T and Bradt R C 1991 *J. Am. Ceram. Soc.* **74** 1296
[23] Ezhilvalavan S and Kutty T R N 1997 *Mater. Chem. Phys.* **49** 258
[24] Gale J 1997 *J. Chem. Soc., Faraday Trans.* **93** 629
[25] Payne M C, Teter M P, Allan D C, Arias T A and Joannopoulos J D 1992 *Rev. Mod. Phys.* **64** 1045
[26] Hohenberg P and Kohn W 1964 *Phys. Rev.* **136** 864B
[27] Kohn W and Sham L 1965 *Phys. Rev.* **140** 1133A
[28] Vanderbilt D 1990 *Phys. Rev.* B **41** 7892
[29] Perdew J, Chevary J, Vosko S, Jackson K, Pederson M, Singh D and Fiolhais C 1992 *Phys. Rev.* B **46** 6671A
[30] Monkhorst H and Pack J 1976 *Phys. Rev.* B **12** 5188
[31] Potin V, Ruterana P, Nouet G, Pond R and Morkoc H 2000 *Phys. Rev.* B **61** 5587
[32] Vitek V, Sutton A P, Wang G J and Schwartz D 1983 *Scr. Metall.* **17** 183
[33] Duke C B, Meyer R J, Paton A and Mark P 1978 *Phys. Rev.* **18** 4225
[34] Schroer P, Kruger P and Pollmann J 1994 *Phys. Rev.* B **49** 17092